Available online at www.sciencedirect.com
ScienceDirect
Journal of Membrane Science 299 (2007) 200–210
journal of MEMBRANE SCIENCE
www.elsevier.com/locate/memsci

Investigation of corrugation phenomenon in the inner contour of hollow fibers during the non-solvent induced phase-separation process

Sina Bonyadi, Tai Shung Chung *, William B. Krantz

Department of Chemical and Biomolecular Engineering, National University of Singapore, 10 Kent Ridge Crescent, Singapore 117602, Singapore

Received 19 March 2007; received in revised form 25 April 2007; accepted 28 April 2007
Available online 3 May 2007

Abstract

In this paper by proposing a novel mechanism, we reveal one of the most controversial issues in the hollow fiber fabrication process regarding the instability leading to the deformed cross-section of fibers fabricated through non-solvent induced phase separation. We have analyzed possible instability mechanisms based on our experimental observations and then postulated that the principal instability occurs in the external coagulation bath where the pressure induced in the nascent fiber outer layer as a result of diffusion/convection, precipitation, densification and shrinkage buckles the rigid precipitated polymer shell in the dope and bore fluid interface. In addition, the effect of some spinning conditions such as air-gap distance, bore fluid composition, take-up speed, external coagulant and dope concentration on the final shape of the fiber cross-section have been investigated. The proposed mechanism is in good qualitative agreement with all our observations.

Keywords: Membrane formation; Phase-separation process; Hollow fiber; Corrugated shape; Instability; Buckling; Fiber spinning

1. Introduction

A membrane is a selective barrier between two adjacent phases that separates specific components in them by preferentially transporting some species relative to others [1]. Among different existing geometrical shapes of membranes, hollow fibers are of great interest because of their high surface area per unit volume and ease of module fabrication. Comprehensive reviews on hollow fiber membrane fabrication process can be found in Refs. [2–5]. However, similar to conventional spinning processes, the fabrication of hollow fibers is inherently accompanied by instabilities that can lead to technical problems in the production line or undesirable final products that can increase production costs. Therefore, understanding the nature of these instabilities as well as methods for controlling them is extremely important. However, these subjects have been often treated as proprietary know-how in the membrane industry and rarely openly discussed in the membrane literature.

The major instabilities encountered in fiber spinning are draw-resonance, necking, capillary break-up and irregular fiber cross-section. The first three phenomena are rather similar in nature and lead to fiber breakage during the spinning or a nonuniform cross-sectional diameter along the spun fibers. These instabilities have been investigated theoretically and experimentally by many researchers and a reasonably good understanding of their mechanism and controlling methods has been outlined in the literature. They are mainly attributed to the amplification of small fluctuations in polymer jet flow as a result of drawing or capillary forces. Larson, Petrie and Lipscomb [6–8] have given comprehensive reviews on this subject.

The last type of spinning instability is related to the nonuniform wall thickness and the irregular cross-section of the as-spun hollow fibers. The severe nonuniformity of the fiber wall thickness is considered to be major impediment for some membrane applications. For example, in high pressure-driven membrane processes, the thin regions in the fiber cross-section are considered as mechanically weak points that are easily collapsed. In addition, the reduced inner cross-sectional area may lead to high pressure drop in treatment of liquid streams flowing through the fiber lumen. On the other hand, if a good control of the phenomenon is achieved, it might be possible to purposely create favorable geometries to the spun fibers that can highly enhance the separation performance of the membranes. For example, hollow fibers with wavy inner or outer wall could be

* Corresponding author. Fax: +65 67791936.
E-mail address: chencts@nus.edu.sg (T.S. Chung).

0376-7388/$ – see front matter © 2007 Elsevier B.V. All rights reserved.
doi:10.1016/j.memsci.2007.04.045

preferable because of their high mass transfer area per unit volume. Recently, both Nijdam et al. [9] and Widjojo and Chung [10] fabricated hollow fibers with wavy geometries at their outer surface, while Koros and co-workers [2] and Santoso et al. [11] observed hollow fibers with a wavy inner skin.

Fibers with wavy geometries might potentially help to increase the flow turbulence and reduce concentration and temperature polarizations. Therefore, a more thorough understanding of the governing mechanisms and approaches to controling the wavy phenomenon are of great interest. However, as far as we know, there are very few studies on this subject. Van't Hof [12] observed the deformed inner layer in the polyethersulfone (PES) fibers fabricated for gas-separation applications. He noticed that the addition of solvent or a weaker coagulant to the bore fluid makes the irregularity more pronounced. Borges and co-workers [13] observed the same phenomenon in spun polyetherimide (PEI) and PES fibers. They found that delayed precipitation induced by the addition of a solvent to the bore fluid and increased air-gap distance impeded the deformation of the fiber cross-section. Both of these studies [12,13] attributed the instability to the competitive effects caused by die-swell (which tried to reduce the bore volume) and by bore liquid (which tried to fill out or expand the bore volume). However, this mechanism does not explain some the observations reported in the present paper.

In this paper, we intend to conduct experiments on the corrugation phenomenon using various polymeric materials and to investigate the factors influencing the underlying instability that causes these patterns. We also propose a novel mechanism that is in good qualitative agreement with our new observations. It is believed that the proposed mechanism can be potentially applied to mathematically model and predict the instability, which will be described in a subsequent paper.

2. Experimental

2.1. Materials

Polyacrylonitrile (PAN) and polyvinylidine flouride (PVDF) were used for the fabrication of the hollow fiber membranes. PAN is a highly hydrophilic polymer that is widely used in pressure-driven membrane processes, whereas PVDF is a hydrophobic polymer that has often been used in membrane contactors. We chose these polymers as extreme ranges of hydrophilicity and hydrphobicity in order to have a database for further investigation. PAN was kindly supplied by Profs. J.Y. Lai and H.A. Tsai at Chung Yuan Christian University of Taiwan, while the commercial PVDF Kynar 761 was purchased from Arkema Inc. *N*-Methyl pyrrolidone (NMP) was used as solvent and supplied by Merck.

2.2. Dope preparation

The polymers were dried at 60 °C under vacuum overnight before they were used for dope preparation. Different concentrations of PAN/NMP and PVDF/NMP spinning solutions were prepared by stirring the solutions at 65 °C and ambient temperature, respectively, over a period of 12 h.

The prepared solutions were degassed overnight before they were used for spinning. The viscosity of the solutions was measured using an ARES Rheometric Scientific Rheometer with a 25 mm cone and plate at ambient temperature.

2.3. Fiber spinning

The hollow fibers were prepared by both wet-spinning and the dry-jet wet-spinning processes using the spinning system described elsewhere [14,15]. The discharged flow of polymer solution and bore fluid passed through air-gap distances ranging from 0 to 20 cm depending on the experimental conditions before entering the external coagulation bath. To investigate the effect of air-gap and bore fluid composition, for each bore fluid composition we tried different air-gap distances. In addition, to investigate the effect of take-up speed, we varied the take-up speed from a low value at which only gravitational force acted in the axial direction to a high value while other conditions remained constant. Moreover, PAN/NMP solutions with different concentrations and viscosities were used in order to study the effect of viscosity and concentration. The details of the spinning conditions for the experiments can be found in Table 1. The as-spun fibers were immersed in water for approximately 2 days for solvent exchange. In order to remove the residual solvent, fibers were immersed in methanol twice, each time for 30 min. The same treatment was carried out using hexane. Afterwards, the fibers were dried by air at room temperature.

2.4. Morphology study of hollow fibers by SEM

Hollow fiber cross-sections were observed by taking SEM pictures using a JEOL JSM-5600LV scanning electron microscope. Fiber samples were immersed in liquid nitrogen, fractured and then coated with platinum using a JEOL JFC-1300 coater.

2.5. Polymer flow observation in the air-gap region by a high magnification camera

By making use of the transparent nature of PAN dope solution we were able to take high magnification pictures of the polymer dope and bore fluid flow geometries in the air-gap region. An EOS 350 digital Canon camera with an MP-E65mm high magnification lens was utilized for the digital visualization.

Table 1
Spinning conditions of hollow fiber membrane fabrication

Parameters	Value
Dope flow rate (ml/min)	2.0
Bore fluid NMP-water (NMP wt. %)	0, 20, 40, 60, 80
Bore flow rate (ml/min)	0.5
Length of air-gap (cm)	0, 3.5, 7, 12, 17, 20
External coagulant	Water, isopropyl alcohol
External coagulant temperature (°C)	25
Spinneret dimensions (mm)	0.85/0.5 (OD/ID)
Spinneret temperature (°C)	25
Take-up speed (ml/min)	Free fall, 404, 515, 626, 737, 848, 958

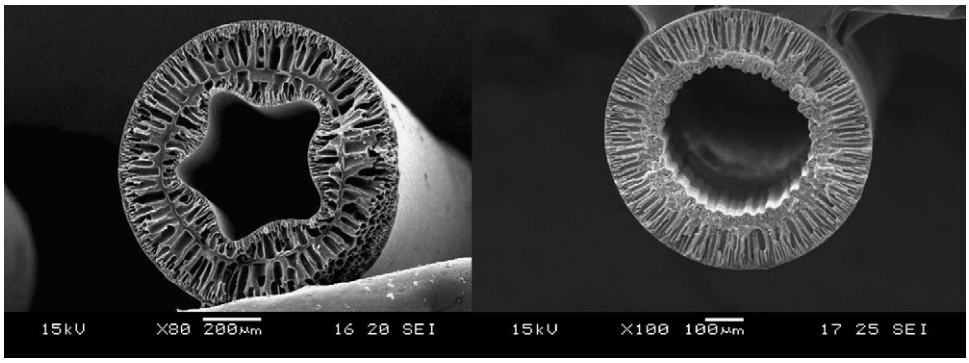

Fig. 1. Irregular shape in the cross-section of the PAN 17% (left) and PVDF 20% (right) hollow fibers fabricated through wet spinning, bore fluid composition of 40% NMP/water (NMP wt.%), free fall take-up rate.

2.6. Video microscopy flow visualization

A drop of dope solution was sandwiched between two microscope slides. Afterwards, a drop of water as a coagulant was introduced to the gap between the two slides by a syringe. The diffusion, precipitation and solidification fronts of water into the dope solution were observed and video-recorded under an Olympus BX50 polarizing optical microscope. These experiments may provide the basic morphological evolution of the phase inversion process.

3. Experimental observations

Fig. 1 shows the cross-section morphology of PAN and PVDF fibers spun through a wet spinning process. It is clearly observable that the inner contour of the fibers is deformed in a way that the wall thickness of the fibers is not uniform circumferentially. In addition, the cross-sectional view of different sections along the fiber shows that the deformation had a similar shape all along the fiber. This shows that in contrast to draw-resonance, the instability is not axially periodic and occurs consistently throughout the spinning process.

The effect of the air-gap distance on macroscopic morphology of the fibers was investigated. The SEM micrographs in Fig. 2 shows the cross-section of the spun PAN hollow fibers for different air-gap distances ranging from 0 to 20 cm. It is observed that by increasing the air-gap distance, the number of corrugations in the inner contour of the fibers decreases from 5 (in the zero air-gap) to 1 corresponding to a circle (in the 20 cm air-gap). In another experiment with no air-gap, we observed that by increasing the solvent concentration in the bore fluid from 0 to 60% the number of corrugations in the inner layer increases from 2 to 8. However, by further increasing the solvent concentration to 80% no deformation is observable (Fig. 3). The same trend was observed for higher air-gaps. In addition, we observed that by replacing a strong external coagulant such as water with a weaker one such as IPA, while keeping other conditions unchanged, no deformation was observed in the cross-section of fabricated fibers. The SEM micrographs in Fig. 4 shows this behavior. The effect of take-up speed was also investigated. The SEM micrographs in Fig. 5 shows that by increasing the take-up speed at a constant air-gap distance, the number of waves increased at first from 3 to 4. However, by further increasing the take-up rate, it decreased so that a circular cross-section appeared ultimately. Finally, we observed that by increasing the dope concentration from 13 to 17 and 22 wt.%, the number of waves decreased from 6 to 4 and 1, respectively. The SEM micrographs in Fig. 6 shows this trend.

The same experiments were carried out using a PVDF dope solution and very similar trends but with different number of waves were observed in these experiments. Fig. 7 shows the

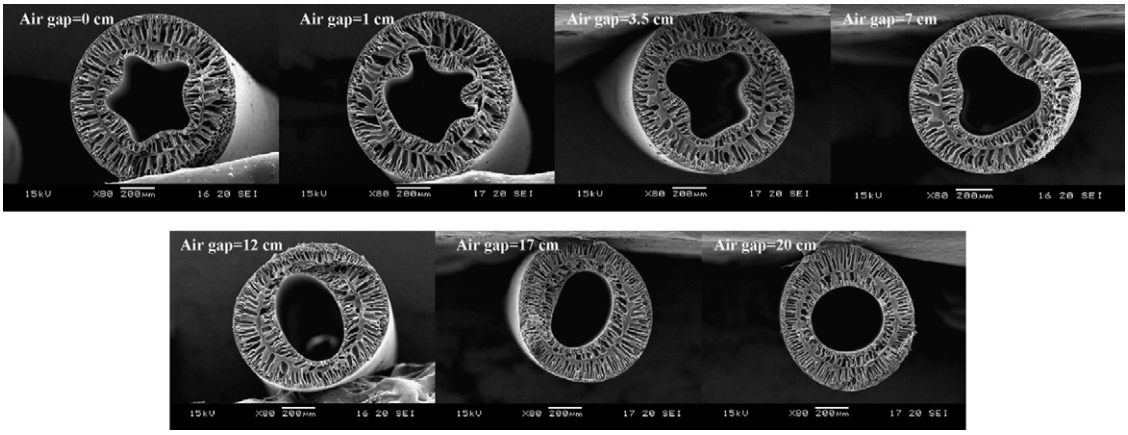

Fig. 2. Cross-section of spun fibers from 17 wt.% PAN solution, 40 wt.% NMP Bore fluid with different air-gap distances.

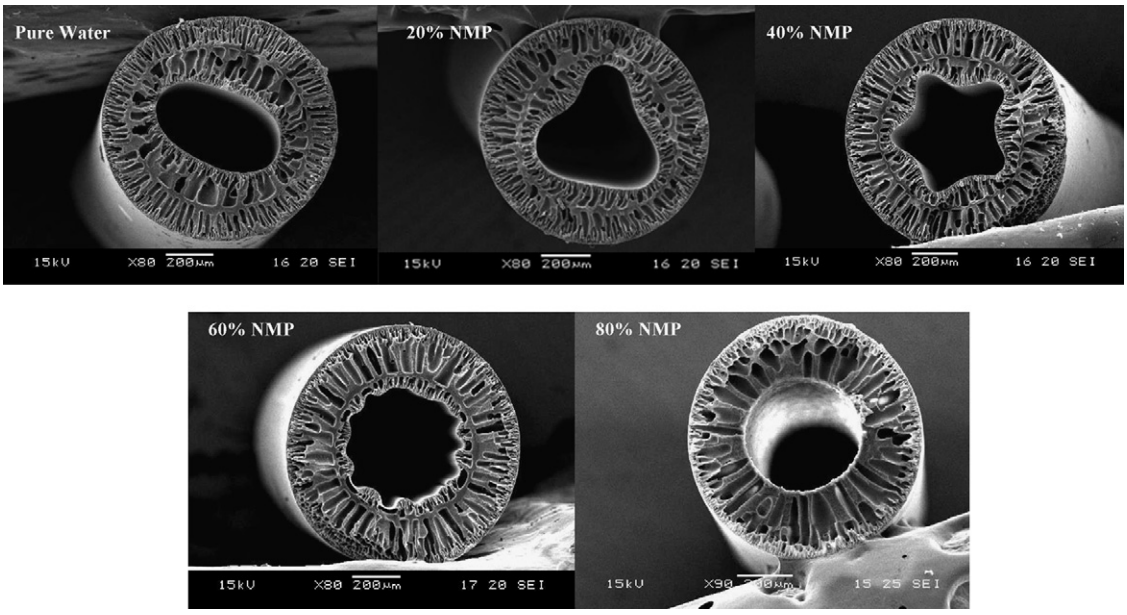

Fig. 3. Cross-section of wet spun fibers from 17 wt.% PAN solution with different solvent amount in the bore fluid.

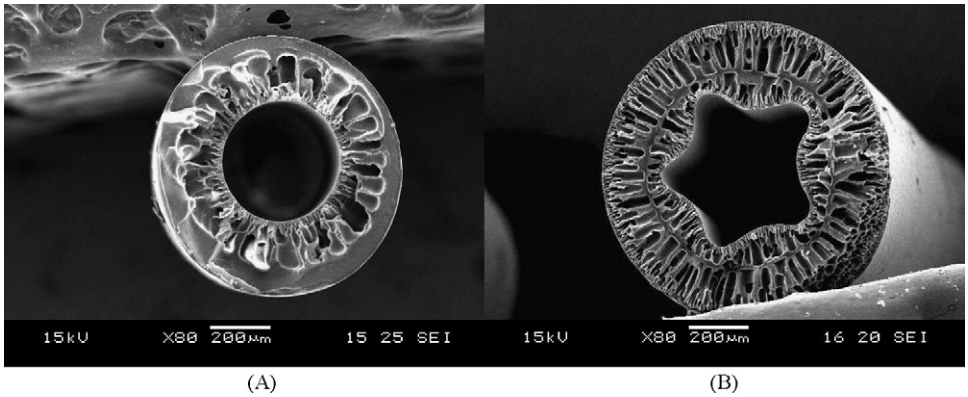

(A) (B)

Fig. 4. Cross-section of wet spun fibers from 17 wt.% PAN solution and 40 wt.% NMP bore fluid using different external coagulants: (A) IPA and (B) water.

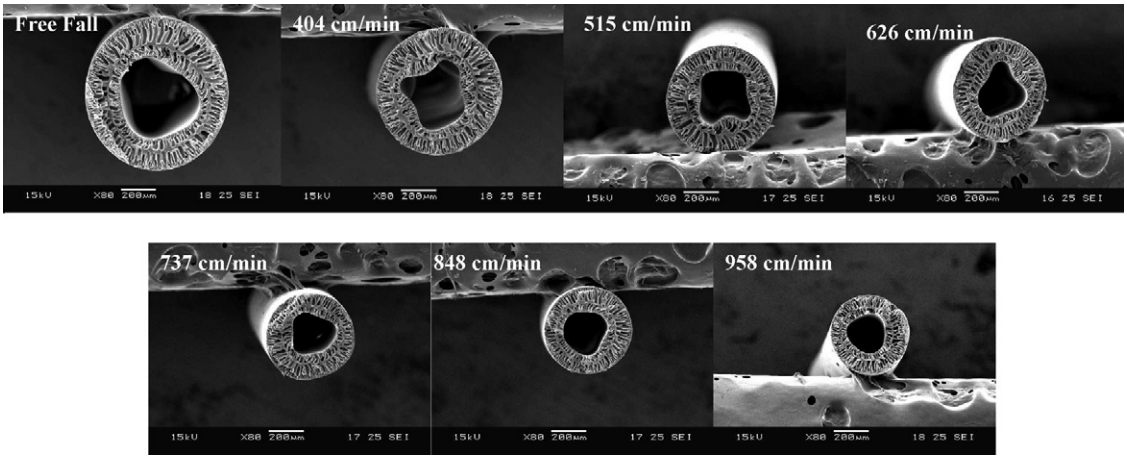

Fig. 5. Cross-section of spun fibers with different take-up rates from 17 wt.% PAN solution, 40 wt.% NMP bore fluid, 7 cm air-gap.

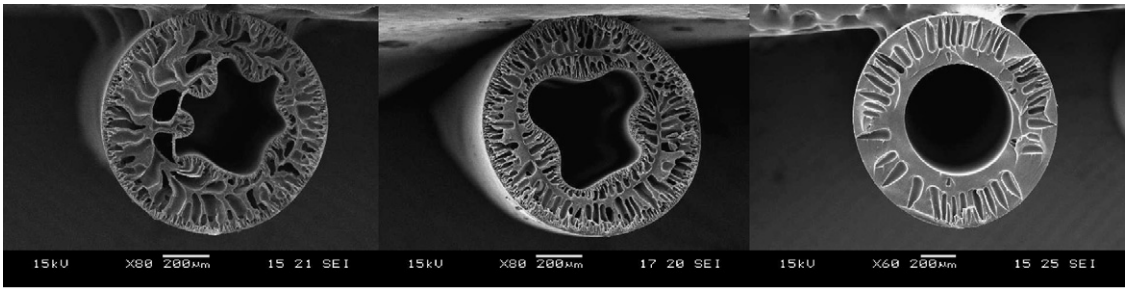

Fig. 6. Cross-section of spun fibers from different concentrations of PAN solution, 40 wt.% NMP aqueous mixture as bore fluid, with 3.5 cm air-gap and free fall: (A) 13 wt.% PAN solution, (B) 17 wt.% PAN solution and (C) 22 wt.% PAN solution.

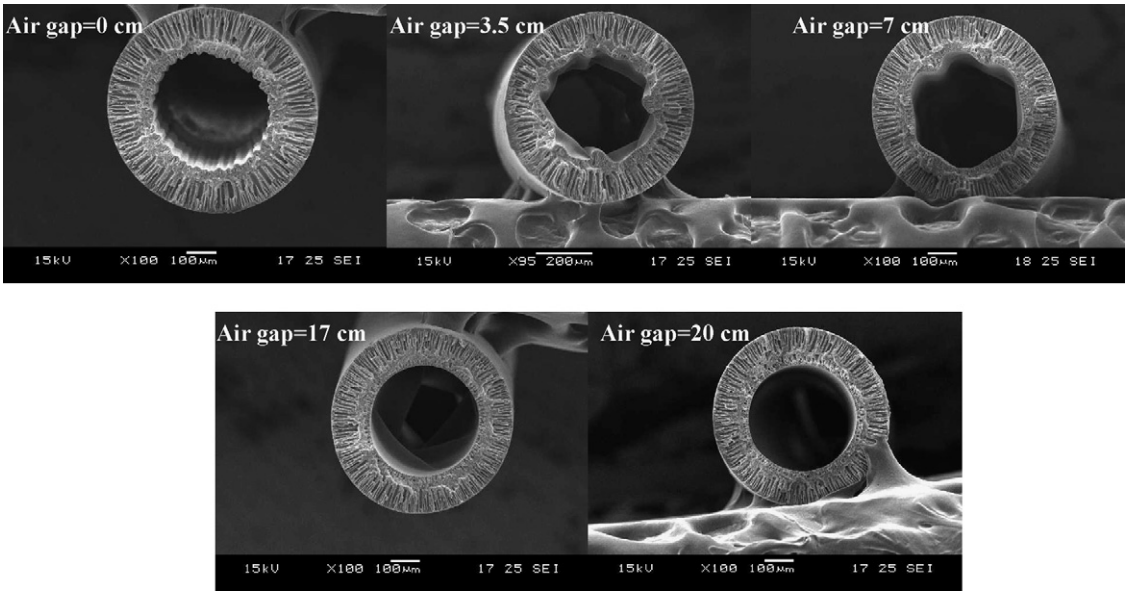

Fig. 7. Cross-section of spun fibers from 20 wt.% PVDF solution, 40 wt.% NMP Bore fluid with different air-gap distances.

effect of air-gap distance on the corrugation of PVDF fibers as an example.

4. Theory

To propose a suitable mechanism for our observations, we tried to find out in which step of the fiber-fabrication process the instability arises. The cross-sectional micrographs of as-spun fibers in Fig. 8 shows that the deformation happens in the fiber-spinning line. Therefore, the deformation cannot be attributed to the drying or post-treatment stages of the fiber fabrication. Previous studies [12,13] postulated that the competitive flow direction between dope solution and bore fluid in the die-swell region is the responsible for this phenomenon. In order to evaluate this hypothesis, we took pictures with high magnifications at the die-swell region. Because of the translucent nature of the PAN solution, we could observe the flow interface between the dope and the bore fluid in the die-swell region. The pictures in Fig. 9 shows the two-phase flow of the PAN solution and the bore fluid after discharging from the spinneret. The location of the interface between the two streams agrees with the spinneret dimensions used in the spinning. Therefore, we confirm that

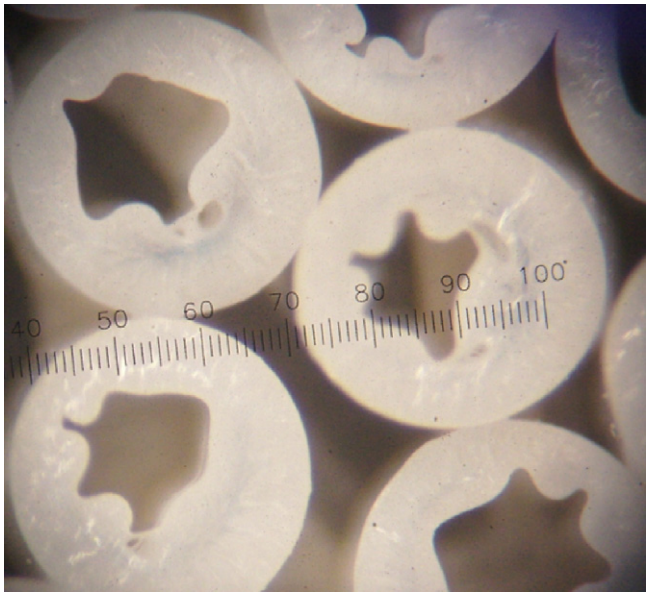

Fig. 8. Cross-section of wet as-spun hollow fibers from 17 wt.% PAN solution and bore fluid containing 40 wt.% NMP.

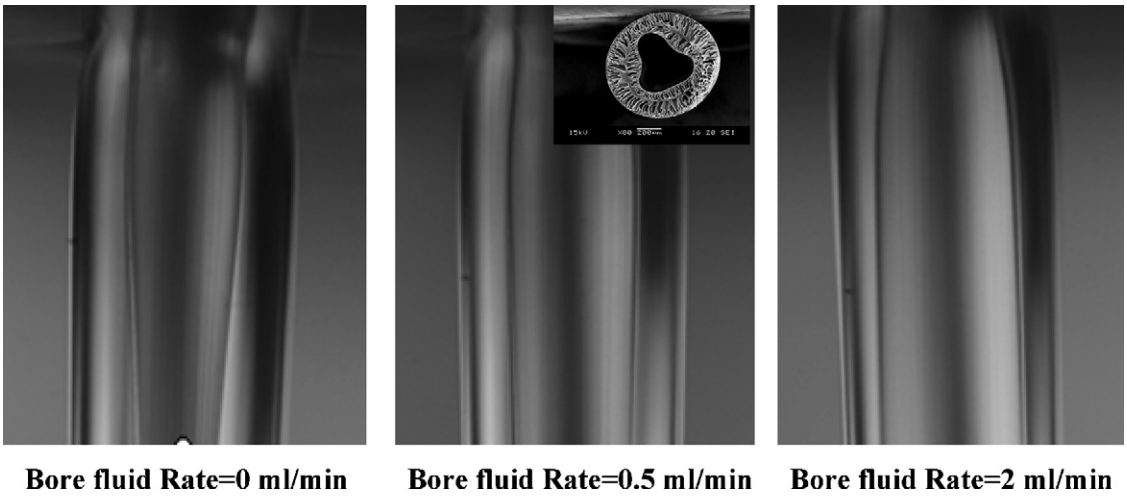

Fig. 9. Magnified die swell pictures of spinning with 17 wt.% PAN solution, Bore fluid containing 40 wt.% NMP and 7 cm air-gap distance, different bore flow rates.

the interface observed in the pictures is not affected by light scattering. These pictures show that the interface between the two streams is not corrugated. Therefore, other factors might be responsible for the instability rather than the competitive force between the dope and the bore fluid.

4.1. System description

As polymer dope discharges from the spinneret and contacts with the bore fluid in the die-swell region, the solvent–non-solvent exchange between the bore fluid and dope flow leads to the formation of three phases in the nascent fiber during the dry-jet wet-spinning. Using flow visualization photos taken from the video microscopy on a flat membrane inversion as an example, the innermost phase, shown as I_1 in Fig. 10, is formed as a result of vitrification induced by the bore fluid. The intermediate phase I_2 lies between the solidification and precipitation fronts. In this region, the solution divides into polymer-lean phase and polymer-rich phases either by nucleation and growth of the polymer-lean phase or by spinodal decomposition. The third region is between the precipitation and diffusion/convective fronts where macrovoids propagate and grow [16,17]. The pictures in Fig. 10(A) clearly show the solidification, precipitation and diffusion/convective fronts and the regions associated with them.

4.1.1. Phases I_1, I_2 or O_1, O_2

Because of the rapid precipitation of polymer in I_1 and I_2 (or O_1 and O_2) phases, they can be approximated as one pseudo homogeneous elastic cylindrical shell, I_s. Therefore, Von Karman elasticity theory will govern the mechanical behavior of this phase [18].

4.1.2. Phase I_3 or O_3

Since this phase is not fully solidified, we treat it as a viscoelastic fluid with varying density and rheology that progress

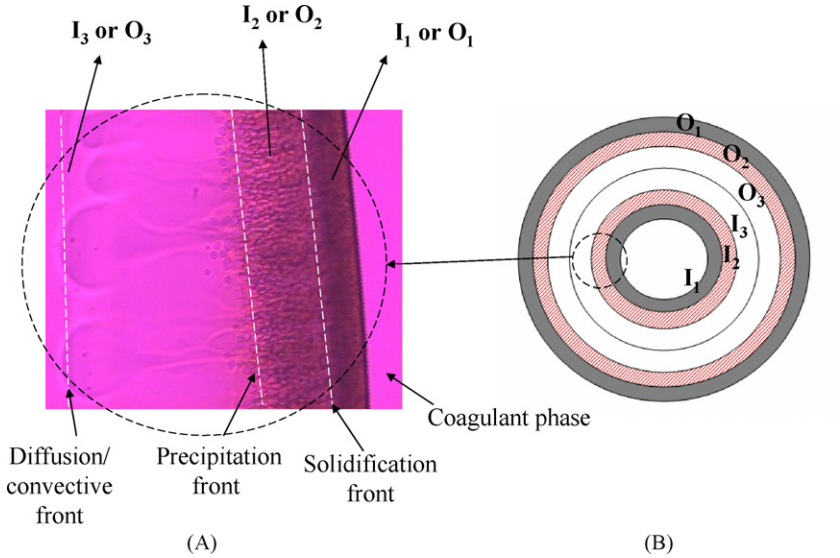

Fig. 10. (A) Penetration of coagulant into the casting solution after 0.2 s using flow visualization photos taken on flat membrane inversion as an example, (B) schematic regions in the extruded nascent fiber.

with the solvent–non-solvent exchange between the dope solution and the bore fluid (or the external coagulant for O_3 phase), and the consequent phase separation. For a detailed description of mass transfer in membrane formation one can refer to Refs. [19–21].

Since the total density is changing in this phase the following equations of continuity and motion can be applied. In writing the following equations, we have assumed a convected coordinate system at the velocity of the interface between the dope and the bore fluid with the positive axial coordinate (z) in the flow direction.

$$\frac{\partial \rho}{\partial t} + \nabla \cdot \rho \vec{u} = 0 \quad (1)$$

$$\frac{\partial \rho \vec{u}}{\partial t} + \rho \vec{u} \cdot \nabla \cdot \vec{u} = -\nabla \cdot P - \nabla \cdot \underline{\underline{\tau}} \quad (2)$$

where ρ is the total density, $\vec{u}$ the velocity vector (u_r, u_θ, u_z), t the time, P the hydrodynamic pressure and τ is the stress tensor. According to the continuity equation (1), velocities are induced in the r, θ and z directions as a result of density change, die swell, non-uniform progresses of diffusion/convective fronts, and rapid precipitation and densification. Therefore, in the corresponding equation of motion (2), a pressure term has to be introduced in order to balance the momentum convection and accumulation terms in the left-hand side of this equation. In a simplified explanation, pressure is generated in this phase mainly as a result of density change.

4.2. Possible instability mechanisms

As it was mentioned before, our system involves elastic, hydrodynamic, mass transfer and solidification phenomena. Therefore, the instability could arise from any of these processes. In the following we analyze the possibility of these mechanisms according to our experimental observations.

A pure hydrodynamic instability such as those observed in polymeric flows, which mostly initiate from nonlinear viscoelastic behavior of polymer solutions or viscosity stratifications in two-phase flows is probably not responsible for the observed instability shown in Figs. 2–7. The strong evidence for this argument is the important effect of the bore fluid composition on the instability. The results section indicated that different deformations of spun fibers were observed depending on the solvent amount in the bore fluid, which translates into a different mass transfer driving force. On the other hand, it is known that the density and viscosity of the NMP as the solvent are very close to those of water. Therefore, it seems that the effect of mass transfer, convective flow and solidification must be taken into account in the stability analysis.

Hence, one possibility is the initiation of an instability that arises from the combined hydrodynamic, mass transfer, convective flow and phase-separation processes. In the following, we describe this possible mechanism qualitatively.

4.2.1. Hypothesis 1 (mass transfer and hydrodynamic instability)

In this hypothesis, the principal instability is described by the equations of continuity, motion and mass transfer in phase I_3, assuming negligible resistance by the elastic cylindrical shell in phase I_s. This assumption is probably valid if the instability occurs very fast before the rigidity of the elastic shell in the interface between the bore fluid and the dope becomes so high. In this case the perturbations occurring in the interface will divide the polymer solution matrix into some regions with different penetration and contact area with the bore fluid. As shown in Fig. 11, the regions associated with the inward movement of the interface have a deeper penetration and increased contact area with the bore fluid. As a result, the solvent–non-solvent exchange rate between the dope and bore fluid will be faster and the pressure induced by precipitation/densification in these regions will be higher compared to the other regions. Subsequently, the generated pressure in regions associated with inward movement would favor the deformation until a new stable state is reached.

This hypothesis provides a good explanation for the instability initiation. However, it is believed that without a strong hoop shrinkage force resulting from the solvent–non-solvent exchange between the dope flow and the external coagulant, and if the dominant motion and force are in gravity direction,

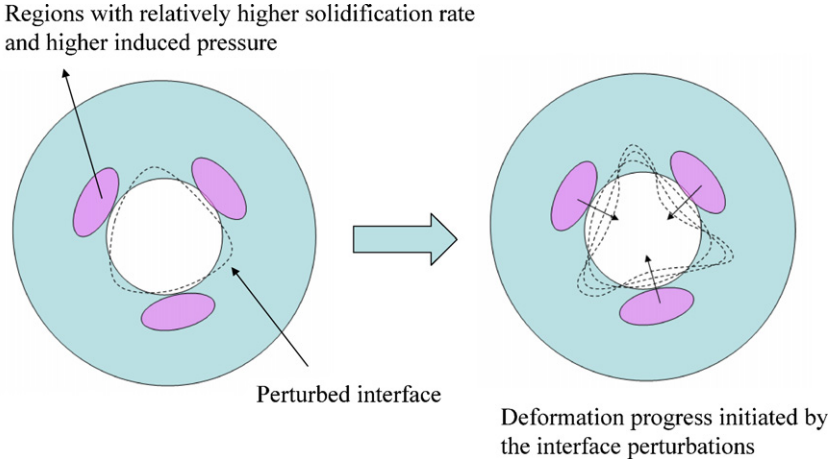

Fig. 11. Instability associated with proposed hydrodynamic and mass transfer mechanism.

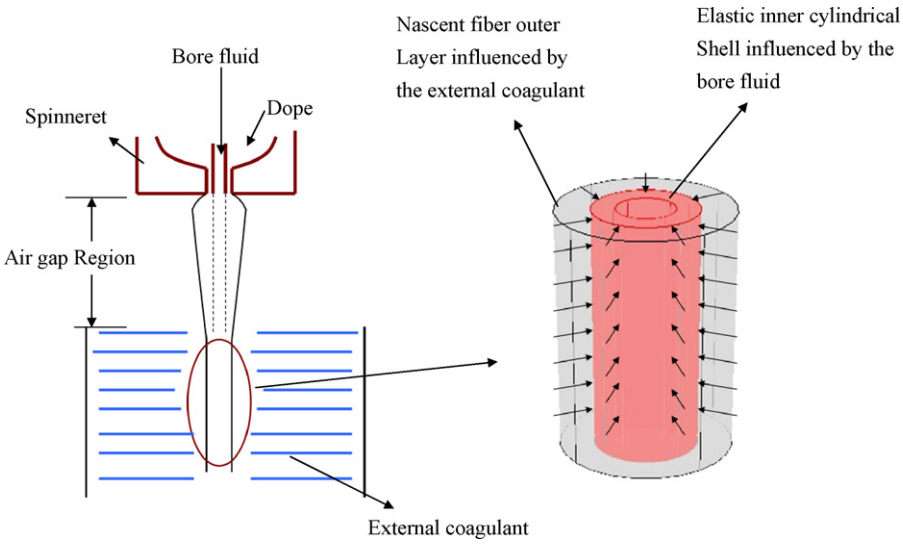

Fig. 12. Schematic picture showing the exertion of inward radial forces generated by the shrinkage of nascent fiber outer layer in the external coagulation bath.

the initial instabilities may not be able to grow significantly. This argument is in agreement with our observations in Figs. 4 and 9, which show no corrugation occurrence in case of a weak external coagulant and in the air-gap region respectively. Therefore, we postulate that the initial instabilities occurring as a result of densification induced pressure in phase I_3 will be magnified in the external coagulation bath by polymer shrinkage and exponentially growth of the dope solution density, while a higher viscosity can be considered as a stabilizing factor.

Another possibility is that the elasticity governs the instability, which will be discussed in the next section as our second hypothesis.

4.2.2. *Hypothesis 2 (elastic and buckling instability)*

In this hypothesis, the principal instability is attributed to the buckling of the elastic cylindrical shell in phase I_s, rather to a hydrodynamic instability. We postulate that the instability occurs in the external coagulation bath where the inward radial force resulting from the shrinkage of the dope outer layer and the density-induced pressure in regions I_3 and O_3 exceeds the critical buckling pressure of the elastic cylindrical shell in phase I_s (defined in Section 4.1.1). Therefore, the instability can be reduced to the buckling of a thin elastic cylindrical shell in the interface between the bore fluid and dope solution under a uniform external pressure. This assumption is probably valid if the resistance by the elastic polymeric shell in phase I_s becomes dominant. Fig. 12 shows this mechanism schematically.

The stability of a long elastic cylinder under external pressure was first studied by Levy [22]. He reduced the stability problem to an algebraic equation involving elliptic integrals and described the critical pressure required for buckling by the following equations:

$$P^* = (k^2 - 1)\frac{B}{R^3} \tag{3}$$

$$B = \frac{Gh^3}{12(1 - v^2)} \tag{4}$$

In the above equations P^* is the buckling critical pressure, B the flexural rigidity, G the Young's modulus, h the thickness of phase I_s, v the Poisson's ratio and k is the buckling mode or the number of circumferential waves observed in the postbuckling shape. Later, using elastic theory, Greenhill [23] integrated the post-buckling shapes corresponding to each equilibrium state. Fig. 13 shows these shapes corresponding to buckling modes 2–5. It is observable that these shapes agree very well with the

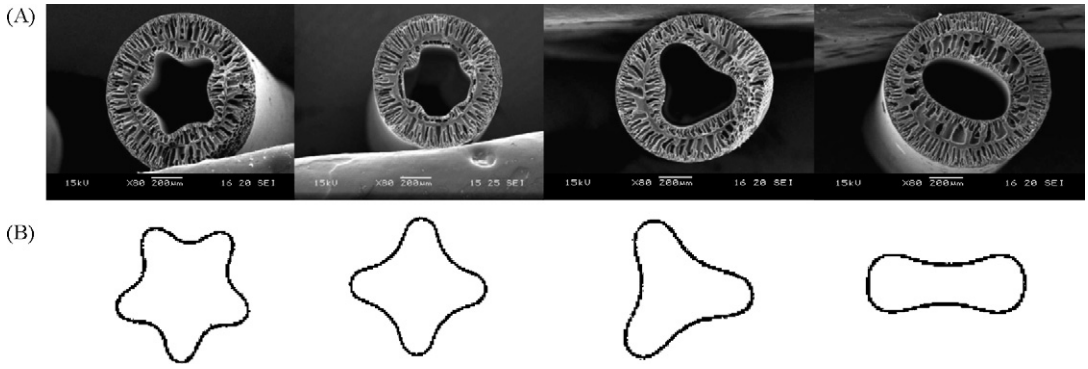

Fig. 13. Close agreement between the spun fibers cross-sectional geometry (A) and the predicted postbuckling shapes of a long elastic cylindrical shell (B).

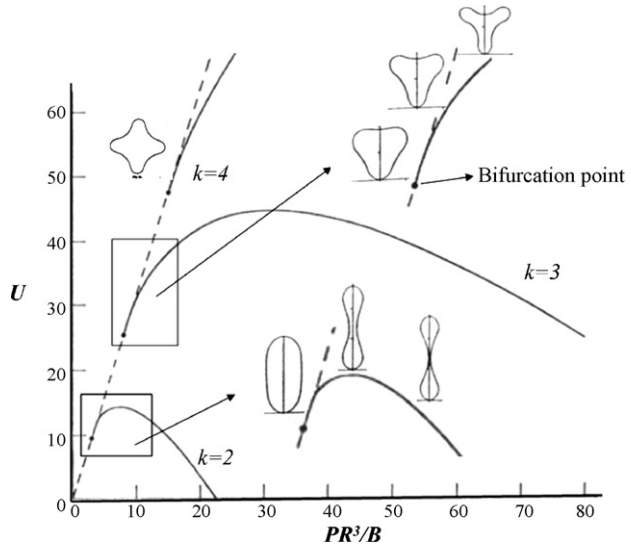

Fig. 14. Energy as a function of the dimensionless group including the external pressure for various modes of deformation.

cross-section of our spun fibers. Fig. 14 shows the energy of an elastic cylinder as a function of system variables for various buckling modes as proposed by Tadjbakhsh and Odeh [24]. This figure shows that as the pressure increases, the energy of the system increases until it reaches a critical bifurcation point at which the equilibrium path changes its stability and divides into some stable and unstable branches.

It is worthy to note that the spinneret eccentricity, non-uniform rigidity of the inner precipitated shell as a result of non-uniform formation of macrovoids and the initial small deformations by the mass transfer-hydrodynamic instability in the air-gap region may lead to the deviation of the fibers cross-sectional shapes from those theoretically predicted in Fig. 13(B).

In the following sections, we explain our observations through the proposed hypotheses.

4.3. Effect of air-gap distance

One possible reason for this trend is that by increasing the air-gap distance, there will be a longer contact time as well as greater solvent exchange between the bore fluid and the dope flow before entering the coagulation bath. As a result, the elastic cylindrical shell in phase I_s may become more rigid, phase I_3 may become more viscous and the initial instabilities may be damped out during the air-gap region at a point in the external coagulation bath where the radial inward shrinkage force is exerted. In addition, for higher air-gaps the cross-sectional area of the dope flow decreases before it enters the coagulation bath. Therefore, the precipitated shell radius, R, in the inner contour of the fiber decreases accordingly. Each of these factors decreases the tendency for the instability to occur. The combination of the mentioned factors could be responsible for the decreasing trend in the corrugation numbers or buckling modes associated with the elastic shell as the air-gap distance increases. Fig. 15 illustrates the relationship between P^*R^3 and the flexural rigidity B as a function of buckling mode k and shows the stable and unstable regions corresponding to Eq. (3). The transitional path of the shell equilibrium states as a function of air-gap distance is shown qualitatively by the symbol of circles in this figure.

4.4. Effect of bore fluid composition

As the solvent amount in the bore fluid increases, the inner nascent fiber becomes less viscous and the flexural rigidity of the inner elastic shell decreases accordingly. Therefore, assuming a constant external pressure, the corrugation mode is expected to increase. However, in spinning with a bore fluid containing about 80 wt.% NMP, no nascent solidified inner layer is formed. In addition, the mass transfer driving force may not be high enough to create the initial instabilities. As a result corrugation does not happen for this condition and the cross-section maintains a circular shape.

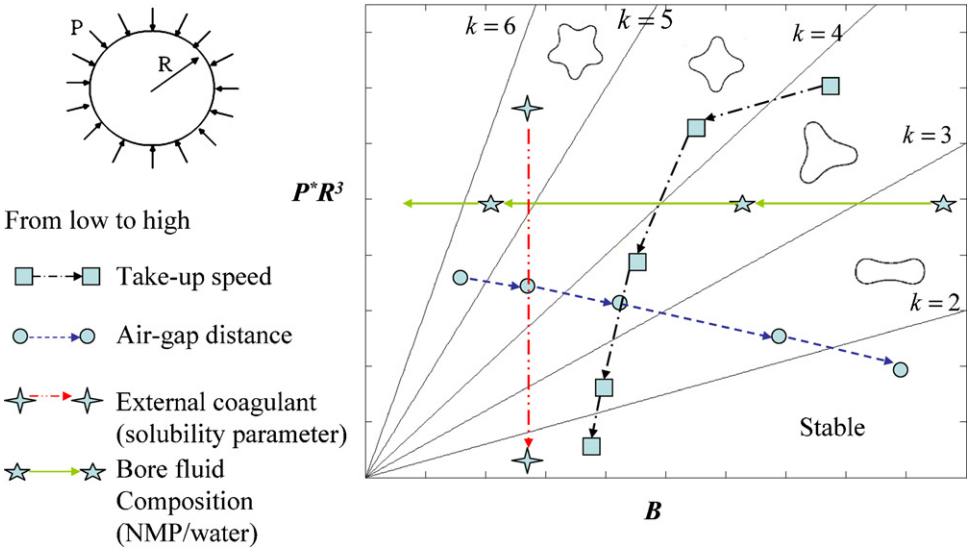

Fig. 15. Equilibrium state transitions of the buckled elastic shell as a function of spinning conditions.

4.5. Effect of external coagulant

The fact that using a weak external coagulant such as IPA inhibits the instability might be due to the fact that a weak coagulant induces a slower solvent exchange, diffusion/convection flows, densification rate and shrinkage which lead to a lower induced external pressure. Therefore, the induced inward radial force could be lower than the critical force required to buckle the elastic shell in phase I_s or amplify the initial instabilities in phase I_3.

4.6. Effect of take-up speed

The increasing and subsequent decreasing trend in corrugation mode as a function of take-up speed can be explained as follows: a higher take-up rate translates into a shorter contact time and solvent exchange between the bore fluid and the dope flow in the air-gap region that leads to a less rigid inner elastic shell. This might be the reason for the initial increase of the buckling. However, as the take-up rate increases further, the cross-sectional diameter of the dope flow decreases consequently. Therefore, the rigid elastic shell will have a smaller radius, greater molecular orientation, and consequently greater resistance to buckling. The smaller radius (i.e., smaller R value) and higher molecular orientation (i.e., higher B value) of the elastic shell resulting from higher take-up rates compensates for the shorter contact time between the bore fluid and the dope flow and produces similar and comparable effects that dominate for lower take-up speeds (i.e., mainly higher B value). The square symbol in Fig. 15 shows the qualitative instability path associated with the inner elastic shell as a function of take-up rate.

4.7. Effect of dope concentration

The stabilizing effect of higher concentration or higher viscosity of the spinning solution may be due to the fact that the rigidity and chain orientation of the inner precipitated shell could be higher for a concentrated dope compared to a dope with a low concentration. As a result, there is less mass transfer-hydrodynamic instability and the inner shell with a higher rigidity will be more resistant to buckling.

5. Conclusion

In this paper, we systematically analyzed the possible mechanisms for the instability occurring in hollow fiber fabrication process leading to the nonuniform cross-section of hollow fibers. Because it takes only a fraction of second for a nascent fiber traveling through the air-gap region, the hydrodynamic instability may not have enough time to magnify its effects. Therefore, we postulated that the hydrodynamic instability may be the initial stage of causing instability and the elastic and buckling instability is the magnifying stage for the development of nonuniform cross-section of hollow fibers. In other words, the pressure induced in the nascent fiber outer layer as a result of diffusion/convection, precipitation, densification and shrinkage will buckle the rigid elastic shell formed in the interface between the bore fluid and the dope solution. To prove our hypothesis, the effects of key spinning parameters such as air-gap distance, bore fluid composition, take-up rate, external coagulant and dope concentration on the final shape of the fibers cross-section have been conducted and investigated. The proposed hypothesis is in good qualitative agreement with all our observations. More rigorous mathematical analyses on the hypothesized mechanism will be carried out in the future work.

Acknowledgements

The authors would like to thank Prof. J.Y. Lai at Chung Yuan Christian University and Prof. H.A. Tsai at Nan Ya Institute of Technology of Taiwan for the provision of PAN resins. Thanks are also to A*STAR and National University of Singapore (NUS) for funding this project with the grant number of R-279-000-218-305.

Nomenclature

B	flexural rigidity (Pa m^3)
G	Young's modulus of elasticity (Pa)
h	shell thickness (m)
k	buckling mode
P	dynamic pressure (Pa)
P^*	critical buckling pressure (Pa)
r	radial coordinate (m)
R	cylinder radius (m)
t	time (s)
$\vec{u}$	velocity vector (m/s)
U	potential energy (kg m/s^2)
v	Poisson's ratio
z	axial coordinate (m)

Greek letter

θ	angular coordinate
ρ	density (kg/m^3)
$\underline{\underline{\tau}}$	viscous flux (Pa)

References

[1] M. Ulbricht, Advanced functional polymer membrane, Polymer 47 (2006) 2217.
[2] S.A. McKelvey, D.T. Clausi, W.J. Koros, A guide to establishing hollow fiber macroscopic properties for membrane applications, J. Membr. Sci. 124 (1997) 223.
[3] K.Y. Wang, T. Matsuura, T.S. Chung, W.F. Guo, The effects of flow angle and shear rate within the spinneret on the separation performance of poly(ethersulfone) (PES) ultrafiltration hollow fiber membranes, J. Membr. Sci. 240 (2004) 67.
[4] H.A. Tsai, C.Y. Kuo, J.H. Lin, D.M. Wang, A. Deratani, C. Pochat-Bohatier, K.R. Lee, J.Y. Lai, Morphology control of polysulfone hollow fiber membranes via water vapor induced phase separation, J. Membr. Sci. 278 (2006) 390.

[5] Y. Su, G.G. Lipscomb, H. Balasubramanian, D.R. Lloyd, Observations of recirculation in the bore fluid during hollow fiber spinning, AIChE 52 (2006) 2072.
[6] R.G. Larson, Instabilities in viscoelastic flows, Rheol. Acta 31 (1992) 213.
[7] C.J.S. Petrie, M.M. Denn, Instabilities in polymer processing, AIChE J. 22 (1976) 209.
[8] G.G. Lipscomb, The melt hollow fiber spinning process: steady-state behavior, sensitivity and stability, Polym. Adv. Technol. 5 (1994) 745.
[9] W. Nijdam, J. de Jong, C.J.M. van Rijn, T. Visser, L. Versteeg, G. Kapantaidakis, G.-H. Koops, M. Wessling, High performance micro-engineered hollow fiber membranes by smart spinneret design, J. Membr. Sci. 256 (2005) 209.
[10] N. Widjojo, T.S. Chung, The thickness and air-gap dependence of macrovoid evolution in phase-inversion asymmetric hollow fiber membranes, Ind. Chem. Eng. Res. 45 (2006) 7618.
[11] Y.E. Santoso, T.S. Chung, K.Y. Wang, M. Weber, The investigation of irregular inner-skin morphology of hollow fiber membranes at high speed spinning and the solutions to overcome it, J. Membr. Sci. 282 (2006) 383.
[12] J.P. Van't Hoff, Wet spinning of polyethersulfone gas separation membranes, Ph.D. Thesis, Twente University, 1988 (Chapter 2).
[13] C.C. Pereira, R. Nobrega, C.P. Borges, Spinning process variables and polymer solution effects in the die swell phenomenon during hollow fiber membrane formation, Brazil. J. Chem. Eng. 17 (2000) 599.
[14] K.Y. Wang, D.F. Li, T.S. Chung, S.B. Chen, The observation of elongation dependent macrovoid evolution in single- and dual-layer asymmetric hollow fiber membranes, Chem. Eng. Sci. 59 (2004) 4657.
[15] T. Matsuura, Synthetic Membranes and Membrane Separation Process, CRC Press, Boca Raton, 1994 (Chapter 3).
[16] H. Strathmann, K. Kock, P. Amar, R.W. Baker, The formation mechanism of asymmetric membranes, Desalination 16 (1975) 179.
[17] P.S.T. Machado, A.C. Habert, C.P. Borges, Membrane formation mechanism based on precipitation kinetics and membrane morphology: flat and hollow fiber polysulfone membranes, J. Membr. Sci. 155 (1999) 171.
[18] F. Bloom, D. Coffin, Handbook of Thin Plate Buckling and Postbuckling, Chapman & Hall/CRC, 2000 (Chapter 1).
[19] L. Yilmaz, A.J. McHugh, Analysis of nonsolvent–solvent–polymer phase diagrams and their relevance to membrane formation modeling, J. Appl. Polym. Sci. 31 (1986) 997.
[20] L. Yilmaz, A.J. McHugh, Modeling of asymmetric membrane formation. II. The effects of surface boundary conditions, J. Appl. Polym. Sci. 35 (1988) (1967).
[21] S.S. Shojaie, W.B. Krantz, A.R. Greenberg, Membrane formation via the dry-cast process. Part I. Model development, J. Membr. Sci. 94 (1994) 255.
[22] M. Levy, Memoire sur un nouveau cas integrable du probleme de l'elastique et l'une de Ses applications., J. de Math. (Liouville), Seri. 3 10 (1884) 5.
[23] A.G. Greenhill, The elastic curve under uniform normal pressure, Math. Ann. 52 (1899) 465.
[24] I. Tadjbakhsh, F. Odeh, Equilibrium states of elastic rings, J. Math. Ann. Appl. 18 (1967) 59.